Journal of the Optical Society of America B
OPTICAL PHYSICS

Proposed narrowband biphoton generation from an ensemble of solid-state quantum emitters

HEEJEONG JEONG,[1,2,3,*] SHENGWANG DU,[1] AND NA YOUNG KIM[4,5]

[1]Department of Physics, The Hong Kong University of Science and Technology, Clear Water Bay, Kowloon, Hong Kong, China
[2]Institute for Advanced Study, The Hong Kong University of Science and Technology, Clear Water Bay, Kowloon, Hong Kong, China
[3]Currently with Department of Physics, Faculty of Science, University of Malaya, 50603 Kuala Lumpur, Malaysia
[4]Institute for Quantum Computing, Department of Electrical and Computer Engineering, University of Waterloo, Waterloo, Ontario, N2L 3G1, Canada
[5]Perimeter Institute for Theoretical Physics, Waterloo, Ontario, N2L 2Y5, Canada
*Corresponding author: jhj413@gmail.com

Received 10 September 2018; revised 11 January 2019; accepted 15 January 2019; posted 15 January 2019 (Doc. ID 344686); published 14 February 2019

We explore a mechanism for producing time-frequency entangled photon pairs (termed a biphoton) from an ensemble of atom-like solid-state quantum emitters. Four distinct energy levels of the solid-state system render four spin-conserving optical transitions as observed in color centers. This feature opens up the possibility to generate a four-wave mixing biphoton based on an electromagnetic induced transparency (EIT) for long-coherence quantum communication as demonstrated in cold atomic systems. We propose a narrow EIT window below a lifetime-limited linewidth of a SiV^- in diamond, assuming a few hundred MHz. Consequently, the EIT-induced narrowband guarantees biphoton coherence time to be at least a few tens of a nanosecond without a cavity. Assessing the criteria of solid-state parameters applicable to the existing biphoton model from cold atoms will accelerate solid-state biphoton source research. This study shows that a realization of negligible ground state dephasing of a solid-state sample will be a crucial step toward a solid-state biphoton generation for more than a 100 ns time scale with a subnatural atomic linewidth of a few MHz.

https://doi.org/10.1364/JOSAB.36.000646

A narrowband biphoton source is an essential ingredient of quantum communications, especially for long-coherence quantum networks based on quantum entanglement [1,2]. A conventional protocol [3] has been tested based on spontaneous parametric down conversion (SPDC) using a nonlinear crystal [4,5]. For practical implementation, the most challenging issue of the conventional biphoton generation method has been short coherence time less than a pico-second (THz) due to the broadband linewidth of nonlinear crystals. The coherence timescale should be at least more than several nanoseconds, which are longer than detection time resolution. For such a timescale up to tens of nanoseconds, the SPDC nonlinear crystal is located inside an optical cavity, and the paired bandwidth has been decreased by 10 MHz [6–13].

A method to control biphoton pairs could be robust if we further increase the coherence timescale. A longer timescale, for example, secures efficient interaction between the heralded single photon and atomic ensemble, which can engineer an entanglement in a temporally correlated scheme [14]. Recently, easily tunable long-coherence time from 50 to 900 ns has been demonstrated as the first subnatural narrowband entangled photon pair generation by utilizing electromagnetically induced transparency (EIT)-based spontaneous four-wave mixing (SFWM) in a laser-cooled cold atomic ensemble [15]. Compared to the cavity-based narrowband SPDC, the EIT-based SFWM cold atomic technique [15–19] has been developed so that the timescale was increased up to a microsecond order [16]. The longer coherence time compared to detection time is the actual benefit for obtaining a high purity of a single photon [20] if we consider about a nanosecond single photon detection time. However, most of these previous EIT-based SFWM narrowband biphoton studies were done in a magneto-optical trap, which requires bulky, complicated apparatus. For this process to be implemented in a real application, we need miniaturization and the capability for photonic chip integration. A hot atomic biphoton source [21,22] would be the intermediate step for the miniaturization. Up to now, there have been several trials to demonstrate fundamental quantum optics in atom-like solid-state systems, such as rare-earth-doped material [23], a quantum dot [24], a nitrogen-vacancy center in diamond [25,26], or a negatively charged silicon-vacancy center in diamond (SiV^-) [27,28]. Most recently, researchers demonstrated a bright single-photon source using SiV^- embedded nanowire array [29]. The nanowire array might improve light

Corrected 21 February 2019

extraction efficiency, so that the integration of a solid-state quantum light source becomes reliable. However, there has been no research activity toward replacing the atomic ensemble with a new solid-state material for the narrowband biphoton generation.

In this article, we assess criteria to determine parameters for the narrowband biphoton generation from atom-like solid-state emitters, such as quantum dots, nitrogen-vacancy or silicon-vacancy centers in diamond via the EIT-SFWM process. Here, we find a parameter regime to apply the existing biphoton model from a cold atomic ensemble to our proposed solid-state system instead of building a new model that only applies to a solid-state system. The idea is to use an atom-like spectrum of solid-state material, for example, negatively charged silicon vacancy in diamond defect centers (SiV^-). The spectral properties of SiV^- show strong optical transition due to a zero-phonon line (ZPL) near 737 nm with weak phonon sidebands [30]. This approach will be used to realize a bandwidth that is even narrower than the lifetime-limited linewidth of the solid-state sample (a few hundred MHz), as has been previously accomplished in an atomic ensemble by achieving less than a natural linewidth (6 MHz). Although further research for achieving a few MHz narrow linewidths like atomic transitions rather than the currently demonstrated 100 MHz is a requirement in material science, our proposed study will pave the way for the implementation of a narrowband biphoton generator towards silicon-based integrated photonic chips for quantum information processing.

The criteria of biphoton generation in solid-state platforms come from spectra of allowed energy levels, linewidths, dipole moments, and polarizations. Our proposed energy scheme considers a double Λ configuration [15] consisting of four energy levels, two excited states, and two ground states, associated with four peaks in absorption spectrum. Each energy level consists of two degenerate levels under zero B-field [28,30]. The optical transition properties of SiV^- are relevant to low energy gaps that originate from carbon dangling bonds [30].

Figure 1 compares experimental schemes and energy levels of: (a) a cold rubidium (Rb) atomic ensemble [15], and (b) a proposed SiV^- diamond case. For both cases, a counter-propagating pump (736.4 nm, ω_p) and coupling (737 nm, ω_c) fields shining on the sample spontaneously generate Stokes (ω_s) and anti-Stokes (ω_{as}) photon pairs by SFWM in the double Λ energy configuration consisting of an off-resonance Raman scattering and EIT. Differences between the two systems are shown in Figs. 1(a) and 1(b). Compared to 15 nm splitting between excited states in Fig. 1(a), proposed excited states are separated by 0.5 nm in wavelength or 258 GHz in frequency, still providing enough spectral resolution between two Λ configurations. Compared to 3.035 GHz ground splitting in ^{85}Rb or 6.834 GHz in ^{87}Rb atoms, the wide ground state splitting, 46 GHz [28,30], of our proposed scheme is meritorious regarding noise reduction in the biphoton generation.

Broadening of a linewidth Γ_0 is the crucial factor in determining coherence time for biphoton generation. The narrowest linewidth of SiV^- diamond defect centers is less than 100 MHz, 94 MHz, which is almost limited by its lifetime, 1.7 ns [28]. In general, however, SiV^- diamond has about a GHz (FWHM) broadening even at cryogenic temperatures [30]. So, our model considers a 160 MHz broadened line by assuming 1 ns lifetime at low temperature of 4 K, and our goal is to achieve less than 100 MHz biphoton linewidth compared to our proposed 160 MHz in this paper. Note that the subnatural linewidth demonstrated in cold atoms [15] is a linewidth

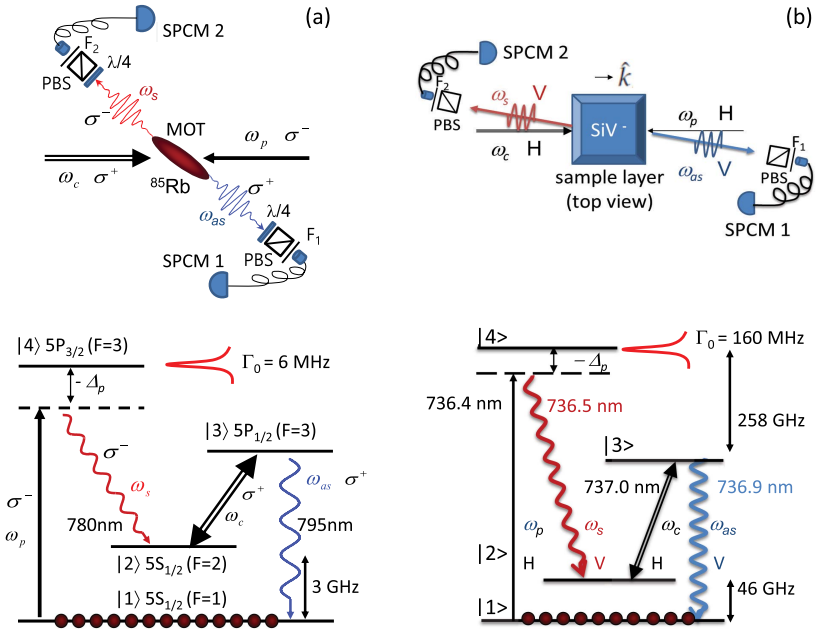

Fig. 1. Schematic diagram of experimental apparatus (top) and double Λ energy levels to generate narrow-band biphotons (bottom) for the case of (a) a cold Rb atomic ensemble [15], and (b) a proposed SiV^- in diamond. Contrary to the circularly polarized driving and generating beams of the cold atomic ensemble, horizontally (H) polarized counter-propagating pump (736.4 nm, ω_p) and coupling (737 nm, ω_c) lasers are shined on our proposed SiV^- to generate vertically (V) polarized counterpropagating phase-matched Stokes (ω_s) and anti-Stokes (ω_{as}) photon pairs. A far-off-detuned pump beam $\Delta_p = 48.67\gamma_{13}$ is the same for both cold atoms and SiV^-. We discuss the details of the energy level in the main text.

narrower than the atomic natural linewidth, 6 MHz. This approach will be directly used, if applicable, for the case of a few MHz narrowband atomic-like solid-state samples when we overcome broadening issues in the future. In contrast to inhomogeneous broadening of atoms depending on temperature (Doppler broadening), spectral broadening in solid-state systems occurs for various reasons: temperature (phonon), crystal symmetry, and strain-induced broadening [31]. Despite the intrinsic strain-induced broadening of heavy atomic defects like N or Si, defect centers show a sharp ZPL. To further reduce the broadening, we consider SiV^- rather than NV in our model because of its D_{3d} crystal structural symmetry [30].

While there are theoretical studies of electronic structure of SiV^- defects using *ab initio* [32], explicit values of dipole moments are not available yet. So, we may extract such values from a measured absorption spectrum. For the case of SiV^-, an optical dipole transition is only allowed for a spin conserving relaxation from excited states to ground states [30].

An empirically determined polarization of each optical transition is characterized by a crystal axis and a converted frame between the lab and internal crystal structure. For example, by a growth technique in sample fabrication stages, one can build a Z-axis ⟨111⟩ oriented SiV^- sample for our proposed linear polarization [30]. Here, we consider a linear dipole moment along the crystal Z axis as vertical (V) polarization, and the other dipole moment confined to the XY plane as horizontal (H) polarization. The set of linear polarizations here meets the SFWM scheme (Fig. 1) similar to our hot atomic biphoton generation [22].

We apply a biphoton model of an atomic system [33] to the SiV^- case. Under the condition of energy consideration, $\omega_c + \omega_p - \omega_{as} - \omega_s = 0$, a biphoton entangled state is given by

$$|\Psi\rangle = L\int \mathrm{d}\omega_{as}\kappa(\omega_{as},\omega_s)\mathrm{sinc}\left(\frac{\Delta kL}{2}\right)\hat{a}_{as}^{\dagger}(\omega_{as})\hat{a}_s^{\dagger}(\omega_s)|0\rangle, \tag{1}$$

where L is medium length, and $\kappa(\omega_{as},\omega_s) = -i(\sqrt{\tilde{\omega}_{as}\tilde{\omega}_s}/2c)\chi^{(3)}(\omega_{as},\omega_s)E_pE_c$ is a nonlinear coupling coefficient. Here, E_p (E_c) is pump (coupling) light amplitude. $\Delta k = (\vec{k}_{as} + \vec{k}_s^{\,*} - \vec{k}_c - \vec{k}_p)\cdot\hat{k}$ describes a phase matching condition and a third-order nonlinear susceptibility related to the four-wave mixing is given by

$$\chi^{(3)}(\omega_{as},\omega_s) = \frac{N\mu_{13}\mu_{23}\mu_{24}\mu_{12}}{4\varepsilon_0\hbar^3(\Delta_p + i\gamma_{14})\left[(\omega + i\gamma_e)^2 - \left(\frac{\Omega_e}{2}\right)^2\right]}. \tag{2}$$

Here, N is the number density of color centers, Δ_p is a pump detuning, μ_{ij} [γ_{ij}] denotes a dipole moment [a dephasing rate] of optical transition between energy levels, $|i\rangle$ and $|j\rangle$, and $\Omega_e = \sqrt{|\Omega_c|^2 - (\gamma_{13} - \gamma_{12})^2}$ and $\gamma_e = (\gamma_{12} + \gamma_{13})/2$ are an effective Rabi frequency and an effective dephasing rate, respectively [33]. We then obtain a biphoton state function $\Psi_{s,as}(t_s,t_{as}) = \psi(\tau)\exp[-i(\tilde{\omega}_s t_s + \tilde{\omega}_{as}t_{as})]$, where $\psi(\tau) = (L/2\pi)\int \mathrm{d}\omega_{as}\kappa(\omega_{as})\Phi(\omega_{as})e^{i\omega_{as}\tau}$ is a two-photon wavefunction, $\Phi(\omega_{as}) = \mathrm{sinc}(\Delta kL/2)e^{i(k_{as}+k_s)\tau}$ is a longitudinal detuning function, $\tilde{\omega}_i$ is a central frequency value, and $\tau = t_{as} - t_s$ denotes a time delay. By considering the atom-like solid-state model as illustrated in Fig. 1(b), we evaluate a biphoton emission rate R (sec^{-1}) as

$$R = \int \mathrm{d}\tau|\psi(\tau)|^2 = \frac{L}{2\pi}\int \mathrm{d}\omega_{as}|\kappa(\omega_{as})\Phi(\omega_{as})|^2. \tag{3}$$

Biphoton coincident counts are proportional to R in Eq. (3). To experimentally demonstrate a heralded single photon pair generation, one needs to confirm nonclassical properties like the violation of the Cauchy–Schwarz inequality [17]. Our proposed scheme here focuses on the level of biphoton generation and the criteria of conventional atomic physics theory applicable to the case of solid-state parameters.

Applying the aforementioned theoretical formalism, we compare parameters of cold Rb atoms as a reference with our proposed parameters for SiV^-, as shown in Table 1. We choose parameters of SiV^- similar to the cold atomic ensemble [15,33] except for the linewidth Γ_0 and ground state dephasing γ_{12}. We assume an ideal situation for SiV^- ensemble as a collection of noninteracting single defects to estimate Γ_0. The ground state dephasing γ_{12} is determined by the spin coherence time $T_s^* \sim 40$ ns in recent coherence population transfer experiments [34,35]. λ_{as} [λ_s] represents a wavelength of an anti-Stokes photon [a Stokes photon]. The ground state splitting is $\Delta_{hf} = 46$ GHz, as described in the beginning. We let $L = 1$ mm for SiV^- as a proposed sample size, which can be extended by an appropriate sample fabrication process, while $L = 1\sim2$ cm for cold Rb atoms. $N = 10^{17}\sim10^{18}$ cm^{-3} is estimated according to 1 ppm, a relatively low defect density but an order of magnitude higher than cold atoms ($N = 10^{16}\sim10^{17}$ cm^{-3}). For the maximum number density case, $N = 10^{18}$ cm^{-3}, the average distance between two emitters is about 10 nm (about 200 Bohr radius) where other effects such as interactions between spins or dipoles are negligible. Consequently, optical depths (OD) are given by $N\sigma_{13}L$, where $\sigma_{13}(= 10^{-14}\sim10^{-13}$ $\mathrm{cm}^2)$ denotes the absorption cross section. An absorption cross section or a dipole moment ($\mu_{13}\times10^{-29}$) of SiV^- can be estimated from absorption or photoluminescence (PL) measurement. Hence, we set σ_{13} and μ_{13} as the same order of cold atomic cases.

Table 1. Comparison of Parameters for Cold Atoms and SiV^-

	Cold Rb Atoms [15,33]		SiV^- [28,30]			
OD	11	53	1.1	11	53	107
λ_{as}	794.76 nm		736.9118 nm			
λ_s	780.24 nm		736.5293 nm			
Δ_{hf}	3.0 GHz		46 GHz			
Γ_0	6 MHz		160 MHz			
γ_{13}	3 MHz		80 MHz			
γ_{12}	$0.6\gamma_{13}$	$0.02\gamma_{13}$	$0.05\gamma_{13}$			
Ω_e	$23.40\gamma_{13}$	$4.09\gamma_{13}$	$4.68\gamma_{13}$			
γ_e	$0.8\gamma_{13}$	$0.51\gamma_{13}$	$0.52\gamma_{13}$			
BW(EIT) [MHz]	247.7	3.64	876.6	277.2	124.0	87.7
BW(PM) [MHz]	412.9	2.76	4676.1	467.6	93.5	46.8

As discussed earlier and shown in Fig. 1, we set a natural linewidth (full-width at half-maximum, FWHM) Γ_0 and a dephasing rate γ_{13} between energy levels 1 and 3. For driving fields, we set the power of a coupling ($P_c = 180$ mW) and a pump laser ($P_p = 3$ mW), and consequently the Rabi frequencies ($\Omega_c = 4.78\gamma_{13}$ and $\Omega_p = 1.45\gamma_{13}$) and the effective Rabi frequency (Ω_e) and effective dephasing rate (γ_e). A far off-detuned pump beam $\Delta_p = 48.67\gamma_{13}$ is a similar condition in a cold atomic case. Finally, to characterize biphoton waveforms in Fig. 2, we list bandwidths (BW) of EIT and a phase matching (PM) that agree with the values in Fig. 3(a).

To begin, we reproduce biphoton waveforms of a reference system (Figs. 2(a), OD = 1.1, and 2(c), OD = 53, of Ref. [33]) by using parameters of cold Rb atoms [15,33] in Table 1. We then evaluate $|\psi(\tau)|^2$ (sec^{-2}) for our proposed SiV$^-$ parameters as in the first row of Fig. 2 for four different OD cases: (a) OD = 1.1, (b) 11, (c) 53, and (d–e) 107. Figures 2(a)–2(b) [(c–e)] show a low OD Rabi oscillatory regime [a high OD group delay regime demonstrating a square-like wave packet]. Although the timescale is only tens of nanoseconds for the SiV$^-$ case, the waveforms are similar to cold atomic cases, especially for high OD [33]. We further investigate the behavior of wavepackets from SiV$^-$ by looking at the spectral properties of each part. We evaluate the biphoton spectrums $|\kappa(\omega_{as})\Phi(\omega_{as})|^2$ in the second row, and anti-Stokes EIT spectrums in the third. Figure 2(a) shows a 2.7 ns period of an oscillatory feature on the biphoton wavepacket corresponding to the distinct two spectral peaks separated by $\Omega_e = 4.68\gamma_{13} \sim 372$ MHz that appears in the second row. Here, the FWHM

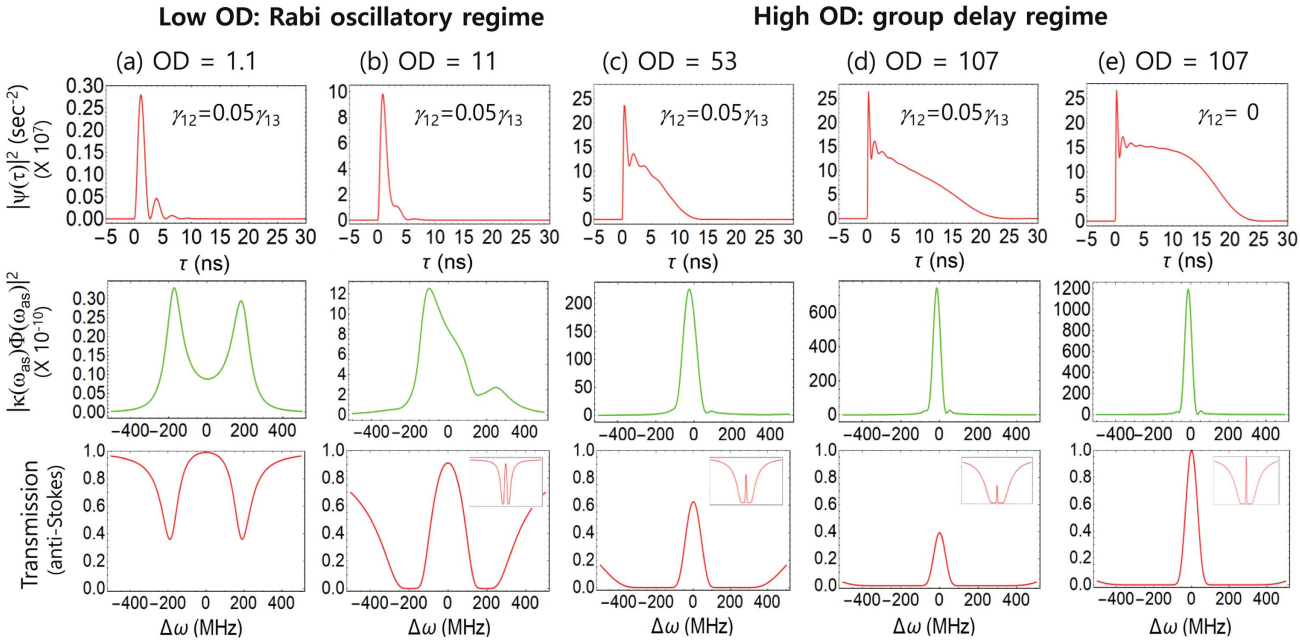

Fig. 2. Temporal and spectral properties of the biphoton generation from the proposed SiV$^-$ parameters in Table 1. The first row shows the biphoton wavepackets $|\psi(\tau)|^2$ (sec^{-2}) as a function of time delay $\tau = t_{as} - t_s$. The second [the third] row shows the biphoton joint spectrum [anti-Stokes EIT spectrum] for (a) OD = 1.1, (b) 11, (c) 53, and (d) 107. Insets show the whole range of the EIT spectrum. Here, $\Omega_c = 4.78\gamma_{13}$ and $\gamma_{12} = 0.05\gamma_{13}$ except for the zero ground dephasing case $\gamma_{12} = 0$ in (e) to show the ideal EIT transmission of unity.

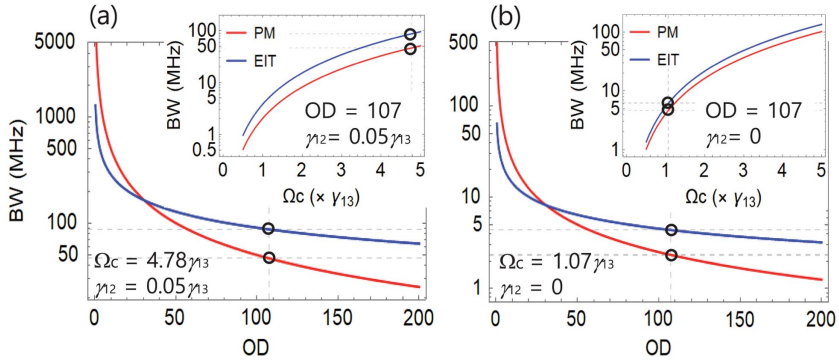

Fig. 3. OD dependant spectral bandwidth (PM and EIT) of biphoton generation in logarithmic scale for (a) $\Omega_c = 4.78\gamma_{13}, \gamma_{12} = 0.05\gamma_{13}$ [Figs. 2(a)–2(d)], and (b) $\Omega_c = 1.07\gamma_{13}, \gamma_{12} = 0$ [Fig. 2(e)]. Insets show BW as a function of coupling Rabi frequency Ω_c. Black circles here show BW values for each parameter sets $[\Omega_c, \gamma_{12}]$ for OD = 107.

linewidth of each spectral sideband agrees with the effective dephasing rate $\gamma_e = 0.52\gamma_{13} \sim 40$ MHz. Both the spectrally wide EIT window and partially absorptive spectrum indicate that the characteristics of the low OD = 1.1.

As we increase the OD, however, two peaks in the biphoton spectrum coalesce to form a single peak at the resonance, especially in the group delay regime [OD > 50, Figs. 2(c)–2(e)]. Consequently, the biphoton spectrum becomes narrower, and the EIT transmission peak decreases due to a non-negligible dephasing γ_{12}. Figure 2(e) shows the case of zero ground state dephasing $\gamma_{12} = 0$ to demonstrate an ideal EIT transmission compared to the $\gamma_{12} = 0.05\gamma_{13}$ case in Fig. 2(d). To investigate $\gamma_{12} = 0$ and Ω_c dependence, we plot EIT [PM] bandwidths in Fig. 3 that are inversely proportional to $\sqrt{\text{OD}}$ [OD] [33]. The PM bandwidth becomes narrower than the EIT for OD > 30 so that, for Fig. 3(a), the EIT [PM] bandwidth becomes 87.7 MHz [46.7 MHz] as shown in Fig. 2(d) and Table 1, which is less than 100 MHz. Note that biphoton spectrum BW agrees well with EIT BW for high OD cases.

To further decrease the EIT bandwidth and eventually achieve below subnatural atomic linewidth in a solid-state sample, we consider a weak coupling $\Omega_c = 1.07\gamma_{13}$ and negligible $\gamma_{12} = 0$ as in Fig. 3(b). Figure 4 shows a group delay time $\tau_d = L/V_g = L(dk_{as}/d\omega)$ at OD = 107 for such a case, which shows a several hundreds nanosecond coherence time of wavepackets, a characteristic of the subnatural linewidth. A realization of nearly zero ground state dephasing $\gamma_{12} = 0$ would be the key to achieve a narrowband below atomic natural linewidth, 6 MHz.

Finally, in addition to our proposed SiV⁻ in the diamond system, we apply our suggested criteria to other solid-state candidates, such as nitrogen-vacancy (NV⁻) defect centers [36,37], germanium-vacancy (GeV⁻) defect centers [38,39], and tin-vacancy (SnV⁻) in diamond [40] as shown in Table 2. SiV⁻, GeV⁻, and SnV⁻ (group IV in the periodic table) with D_{3d} structural symmetry exhibit their sharp spectral properties and the four distinct energy levels compared to the NV defect diamond; consequently, they are the most appropriate candidates. The drawback, however, might be blinking of the fluorescence, which can be improved by the sample growth technique [39]. Although we did not include them in Table 2, quantum dots or hybrid two-dimensional materials can be categorized with various energy schemes of the EIT-SFWM as investigated in the cold atomic system.

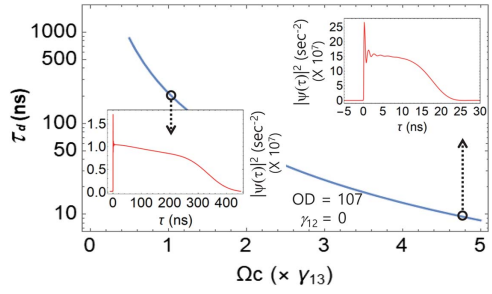

Fig. 4. Group delay τ_d as a function of Ω_c for zero dephasing $\gamma_{12} = 0$ and OD = 107. Insets show that τ_d agrees with coherence timescale in the high OD group delay regime.

Table 2. Parameters for Quantum Emitter Candidates: Nitrogen-Vacancy (NV⁻), Silicon-Vacancy (SiV⁻), and Germanium-Vacancy (GeV⁻) Center of Diamond Defects

	NV⁻ [36,37]	SiV⁻ [28,30]	GeV⁻ [38,39]
λ_{as}	637.199 nm	736.9118 nm	602.54 nm
λ_s	637.189 nm	736.5293 nm	601.54 nm
Δ_{hf}	2.88 GHz	46 GHz	152 GHz
Γ_0	16 MHz	160 MHz	52 MHz
γ_{13}	8 MHz	80 MHz	26 MHz
γ_{12}	1.0–2.4 kHz	4 MHz	9 MHz

In conclusion, we propose the observability of EIT-SFWM based biphoton generation in an atom-like solid-state system, SiV⁻, towards long-distance quantum communication by entangled photons. We find the matching criteria of solid-state biphoton generation from SiV- where we can directly use existing biphoton theory of the cold atomic ensemble. Such criteria include crystal structure affecting the broadening and polarization, crystal axis associated with the polarization condition in SFWM, and the selection rule for an optical transition. In detail, two excited states and two ground states associated with strong optical transitions in SiV⁻ form a double Λ system as a basis of Stokes and anti-Stokes photon pair generation. Spin conserving relaxation from excited states to ground states determines the selection rule for each dipole transition. Under the zero magnetic field, intrinsic light polarizations of the solid-state samples are characterized by the crystal axis, which matches our design of four-wave mixing: H-polarized light for two driving fields and V-polarized light for Stokes and anti-Stokes photons. The main challenge (or difference) of applying the atomic model to solid-state systems is to estimate absolute values of absorption coefficients α_0 and theoretical dipole moments μ_{ij}. Therefore, we consider empirical weights based on existing spectral studies of SiV⁻. Several merits to using solid-state samples include high OD if we overcome the inhomogeneous broadening issues and reduce the ground state dephasing γ_{12} further. Enhanced light coupling efficiency of the nanowire array [29] would be useful in our proposed narrowband biphoton generator. Our proposed EIT-SFWM-based diamond defects photon source is ideal when it is combined with a spin-based memory in a way that photon-driven ground state spin flips, so that the spin state controls biphoton generation for a read-write process of quantum information. Our approach might pave a way toward a 1 μs long coherence time for practical usage of solid-state based quantum communication.

Funding. Research Grants Council, University Grants Committee (RGC, UGC) (16303417); Hong Kong University of Science and Technology (HKUST) (IGN16SC06).

Acknowledgment. H. Jeong acknowledges X. Guo at HKUST for helpful discussions. N. Y. Kim appreciates the support from Industry Canada, and the Ontario Ministry of Research Innovation through Early Researcher Awards.

REFERENCES

1. H. J. Kimble, "The quantum internet," Nature **453**, 1023–1030 (2008).

2. L. M. Duan, M. D. Lukin, J. I. Cirac, and P. Zoller, "Long-distance quantum communication with atomic ensembles and linear optics," Nature **414**, 413–418 (2001).
3. A. K. Ekert, "Quantum cryptography based on bellâs theorem," Phys. Rev. Lett. **67**, 661–663 (1991).
4. S. E. Harris, M. K. Oshman, and R. L. Byer, "Observation of tunable optical parametric fluorescence," Phys. Rev. Lett. **18**, 732–734 (1967).
5. D. Burnham and D. Weinberg, "Observation of simultaneity in parametric production of optical photon pairs," Phys. Rev. Lett. **25**, 84–87 (1970).
6. Z. Y. Ou and Y. J. Lu, "Cavity enhanced spontaneous parametric down-conversion for the prolongation of correlation time between conjugate photons," Phys. Rev. Lett. **83**, 2556–2559 (1999).
7. C. E. Kuklewicz, F. N. C. Wong, and J. H. Shapiro, "Time-bin-modulated biphotons from cavity enhanced down-conversion," Phys. Rev. Lett. **97**, 223601 (2006).
8. X.-H. Bao, Y. Qian, J. Yang, H. Zhang, Z.-B. Chen, T. Yang, and J.-W. Pan, "Generation of narrow-band polarization-entangled photon pairs for atomic quantum memories," Phys. Rev. Lett. **101**, 190501 (2008).
9. M. Scholz, L. Koch, R. Ullmann, and O. Benson, "Single-mode operation of a high-brightness narrow-band single-photon source," Appl. Phys. Lett. **94**, 201105 (2009).
10. G. Y. Y. C.-S. Chuu and S. E. Harris, "A miniature ultrabright source of temporally long, narrow-band biphotons," Appl. Phys. Lett. **101**, 051108 (2012).
11. J. Fekete, D. Rielander, M. Cristiani, and H. de Riedmatten, "Ultranarrow-band photon-pair source compatible with solid state quantum memories and telecommunication networks," Phys. Rev. Lett. **110**, 220502 (2013).
12. Z.-Y. Zhou, D.-S. Ding, Y. Li, F.-Y. Wang, and B.-S. Shi, "Cavity-enhanced bright photon pairs at telecom wavelengths with a triple-resonance configuration," J. Opt. Soc. Am. B **31**, 128–134 (2014).
13. K. Niizeki, M. Ikeda, K. Zheng, X. Xie, K. Okamura, N. Takei, N. Namekata, S. Inoue, H. Kosaka, and T. Horikiri, "Ultrabright narrow-band telecom two-photon source for long-distance quantum communication," Appl. Phys. Express **11**, 042801 (2018).
14. X. Guo, Y. Mei, and S. Du, "Testing the bell inequality on frequency-bin entangled photon pairs using time-resolved detection," Optica **4**, 388–392 (2017).
15. S. Du, P. Kolchin, C. Belthangady, G. Y. Yin, and S. E. Harris, "Subnatural linewidth biphotons with controllable temporal length," Phys. Rev. Lett. **100**, 183603 (2008).
16. L. Zhao, X. Guo, C. Liu, Y. Sun, M. M. T. Loy, and S. Du, "Photon pairs with coherence time exceeding 1 μs," Optica **1**, 84–88 (2014).
17. L. Zhao, Y. Su, and S. Du, "Narrow-band biphoton generation in the group delay regime," Phys. Rev. A **93**, 033815 (2016).
18. M.-X. Dong, W. Zhang, Z.-B. Hou, Y.-C. Yu, S. Shi, D.-S. Ding, and B.-S. Shi, "Experimental realization of narrowband four-photon Greenberger-Horne-Zeilinger state in a single cold atomic ensemble," Opt. Lett. **42**, 4691–4694 (2017).
19. Y. C. Yu, D. S. Ding, M. X. Dong, S. Shi, W. Zhang, and B. S. Shi, "Self-stabilized narrow-bandwidth and high-fidelity entangled photons generated from cold atoms," Phys. Rev. A **97**, 043809 (2018).
20. S. Du, "Quantum-state purity of heralded single photons produced from frequency-anticorrelated biphotons," Phys. Rev. A **92**, 043836 (2015).
21. C. Shu, P. Chen, T. K. A. Chow, L. Zhu, Y. Xiao, M. M. Loy, and S. Du, "Subnatural-linewidth biphotons from a Doppler-broadened hot atomic vapour cell," Nat. Commun. **7**, 12783 (2016).
22. L. Zhu, X. Guo, C. Shu, H. Jeong, and S. Du, "Bright narrow-band biphoton generation from a hot rubidium atomic vapor cell," Appl. Phys. Lett. **110**, 161101 (2017).
23. E. Saglamyurek, J. Jin, V. B. Verma, M. D. Shaw, F. Marsili, S. W. Nam, D. Oblak, and W. Tittel, "Quantum storage of entangled telecom-wavelength photons in an erbium-doped optical fibre," Nat. Photonics **9**, 83–87 (2015).
24. F. Jahnke, C. Gies, M. Aßmann, M. Bayer, H. A. M. Leymann, A. Foerster, J. Wiersig, C. Schneider, M. Kamp, and S. Höfling, "Giant photon bunching, superradiant pulse emission and excitation trapping in quantum-dot nanolasers," Nat. Commun. **7**, 11540 (2016).
25. S. Yang, Y. Wang, D. D. B. Rao, T. H. Tran, A. S. Momenzadeh, M. Markham, D. J. Twitchen, P. Wang, W. Yang, R. Stöhr, P. Neumann, H. Kosaka, and J. Wrachtrup, "High-fidelity transfer and storage of photon states in a single nuclear spin," Nat. Photonics **10**, 507–511 (2016).
26. F. Kong, C. Ju, Y. Liu, C. Lei, M. Wang, X. Kong, P. Wang, P. Huang, Z. Li, F. Shi, L. Jiang, and J. Du, "Direct measurement of topological numbers with spins in diamond," Phys. Rev. Lett. **117**, 060503 (2016).
27. A. Sipahigil, K. D. Jahnke, L. J. Rogers, T. Teraji, J. Isoya, A. S. Zibrov, F. Jelezko, and M. D. Lukin, "Indistinguishable photons from separated silicon-vacancy centers in diamond," Phys. Rev. Lett. **113**, 113602 (2014).
28. L. J. Rogers, K. D. Jahnke, T. Teraji, L. Marseglia, C. Müller, B. Naydenov, H. Schauffert, C. Kranz, J. Isoya, L. P. McGuinness, and F. Jelezko, "Multiple intrinsically identical single-photon emitters in the solid state," Nat. Commun. **5**, 4739 (2014).
29. L. Marseglia, K. Saha, A. Ajoy, T. Schröder, D. Englund, F. Jelezko, R. Walsworth, J. L. Pacheco, D. L. Perry, E. S. Bielejec, and P. Cappellaro, "Bright nanowire single photon source based on SiV centers in diamond," Opt. Express **26**, 80–89 (2018).
30. C. Hepp, T. Müller, V. Waselowski, J. N. Becker, B. Pingault, H. Sternschulte, D. Steinmüller-Nethl, A. Gali, J. R. Maze, M. Atatüre, and C. Becher, "Electronic structure of the silicon vacancy color center in diamond," Phys. Rev. Lett. **112**, 036405 (2014).
31. H. Sternschulte, K. Thonke, P. C. Sauer, R. Münzinger, and P. Michler, "1.681-ev luminescence center in chemical-vapor-deposited homoepitaxial diamond films," Phys. Rev. B **50**, 14554–14560 (1994).
32. A. Gali and J. R. Maze, "Ab initio study of the split silicon-vacancy defect in diamond: electronic structure and related properties," Phys. Rev. B **88**, 235205 (2013).
33. S. Du, J. Wen, and M. H. Rubin, "Narrow-band biphoton generation near atomic resonance," J. Opt. Soc. Am. B **25**, C98–C108 (2008).
34. B. Pingault, J. N. Becker, C. H. H. Schulte, C. Arend, C. Hepp, T. Godde, A. I. Tartakovskii, M. Markham, C. Becher, and M. Atatüre, "All-optical formation of coherent dark states of silicon-vacancy spins in diamond," Phys. Rev. Lett. **113**, 263601 (2014).
35. L. J. Rogers, K. D. Jahnke, M. H. Metsch, A. Sipahigil, J. M. Binder, T. Teraji, H. Sumiya, J. Isoya, M. D. Lukin, P. Hemmer, and F. Jelezko, "All-optical initialization, readout, and coherent preparation of single silicon-vacancy spins in diamond," Phys. Rev. Lett. **113**, 263602 (2014).
36. V. M. Acosta, K. Jensen, C. Santori, D. Budker, and R. G. Beausoleil, "Electromagnetically induced transparency in a diamond spin ensemble enables all-optical electromagnetic field sensing," Phys. Rev. Lett. **110**, 213605 (2013).
37. E. Togan, Y. Chu, A. S. Trifonov, L. Jiang, J. Maze, L. Childress, M. V. G. Dutt, A. S. Sørensen, P. R. Hemmer, A. S. Zibrov, and M. D. Lukin, "Quantum entanglement between an optical photon and a solid-state spin qubit," Nature **466**, 730–734 (2010).
38. M. K. Bhaskar, D. D. Sukachev, A. Sipahigil, R. E. Evans, M. J. Burek, C. T. Nguyen, L. J. Rogers, P. Siyushev, M. H. Metsch, H. Park, F. Jelezko, M. Lončar, and M. D. Lukin, "Quantum nonlinear optics with a germanium-vacancy color center in a nanoscale diamond waveguide," Phys. Rev. Lett. **118**, 223603 (2017).
39. P. Siyushev, M. H. Metsch, A. Ijaz, J. M. Binder, M. K. Bhaskar, D. D. Sukachev, A. Sipahigil, R. E. Evans, C. T. Nguyen, M. D. Lukin, P. R. Hemmer, Y. N. Palyanov, I. N. Kupriyanov, Y. M. Borzdov, L. J. Rogers, and F. Jelezko, "Optical and microwave control of germanium-vacancy center spins in diamond," Phys. Rev. B **96**, 081201(R) (2017).
40. T. Iwasaki, Y. Miyamoto, T. Taniguchi, P. Siyushev, M. H. Metsch, F. Jelezko, and M. Hatano, "Tin-vacancy quantum emitters in diamond," Phys. Rev. Lett. **119**, 253601 (2017).